On the Advance of Perihelia in the Kerr Spacetime

Sajanth Subramaniam

ETH Zurich*

Spring 2018

Abstract

We derive an equatorial effective potential from the Kerr metric and use it to derive an analytical expression for the perihelion shift of a slowly orbiting massive object in the gravitational far-field limit of a slowly rotating black hole. We then argue, that in the appropriate limit, this result also holds for planetary motion around the Sun, in particular for the case of Mercury. We find that the contribution of the Sun's rotation to the Mercurian perihelion shift is $-0.002''$/century which is to be compared with the pure Schwarzschild contribution of $42.9''$/century. In the second part we look at the behaviour of the effective potential in the near-field regime. We will discuss the ergosphere and frame-dragging effects with the help of numerical solutions. Finally, we compute numerical results for the perihelion shift of massive test particles orbiting close to the rotating black hole. In particular we examine the dependence of the perihelion shift on the dimensionless spin parameter a/m of the black hole and the orbit size via the geodesic constant of motion L.

Contents

*This semester thesis was written in the Gravitation and Astrophysics group of Prof. Philippe Jetzer at the University of Zurich

1 Introduction

The Kerr metric is a generalisation of the Schwarzschild metric and describes the vacuum solution of the Einstein field equations for an uncharged, rotating, axial-symmetric black hole. The Schwarzschild solution was discovered shortly after Einstein published the field equations in 1915 by Karl Schwarzschild [1] in the very same year. It was in the following year when Einstein proposed three possible tests to gather observational evidence for the validity of his general theory of relativity [2]. One of them was addressing the known problem of Mercury and its perihelion, namely an observed advance of around $43''$/century which could not be explained by Newtonian gravity. The fact that Einstein's theory was able to explain this deviation was a major step in accepting the general theory of relativity. Although Einstein did use a different approach, the observed perihelion shift can also be calculated directly via the Schwarzschild metric, since it describes the unique exterior solution to any spherical symmetric source (Birkhoff's theorem). The search for other exact solutions of the field equations began, of which a solution to a rotating, axial symmetric source was sought out most eagerly. It was only in 1963 when Roy Kerr [3] discovered such a solution.

2 The Kerr metric and geodesic motion

In this section we will derive a radial equation with an effective potential term (as known from Newtonian celestial mechanics) from the Kerr metric. This will help us understand the radial motion of geodesics in the equatorial plane of the Kerr spacetime and compare it to the Newton/Schwarzschild case.

2.1 Effective potential

The Kerr Metric in Boyer-Lindquist coordinates reads [4]

$$ds^2 = (1 - \frac{2mr}{\Sigma})dt^2 + \frac{4amr\sin^2\theta}{\Sigma}dtd\phi - \frac{\Sigma}{\Delta}dr^2 - \Sigma d\theta^2 - (r^2 + a^2 + \frac{2ma^2r\sin^2\theta}{\Sigma})\sin^2\theta d\phi^2 \quad (1)$$

with $\Sigma = r^2 + a^2\cos^2\theta$ and $\Delta = r^2 - 2mr + a^2$.
Note that we have used natural units with $c = 1$ and $G = 1$. In particular we have

$$c^2dt^2 \to dt^2$$
$$\frac{Gm}{c^2} \to m$$

The Kerr metric has the property of being asymptocially flat in the limit of $r \to \infty$ which allows us to identify the parameter m with the mass of our graviational source and a with the angular momentum J via $J = ma$.

The Lagragian for geodesic motion reads

$$\mathcal{L} = g_{\mu\nu}\dot{x}^\mu\dot{x}^\nu$$

We note that the metric (1) possesses the Killing fields $\frac{\partial}{\partial t}$ and $\frac{\partial}{\partial\phi}$ yielding the following constants of motion

$$\frac{\partial\mathcal{L}}{\partial\dot{t}} = const. \equiv A$$
$$\frac{\partial\mathcal{L}}{\partial\dot{\phi}} = const \equiv B$$

Moreover the Lagrangian itself is conserved since the Hamiltonian of the system coincides with the Lagrangian and $\frac{\partial\mathcal{L}}{\partial\tau} = 0$ with τ being the proper time of the geodesic. In the following we will restrict ourselves to geodesic motion in the equatorial plane $\theta = \pi/2$. Such geodesics exist because of symmetry considerations. Note that in contrast to the Schwarzschild case there is an distinguished equatorial plane perpendicular to the spin axis of the source. In this case we have

$$\begin{aligned}\mathcal{L}_{\theta=\frac{\pi}{2}} &= (1 - \frac{2m}{r})\dot{t}^2 + \frac{4am}{r}\dot{t}\dot{\phi} - \frac{r^2}{\Delta}\dot{r}^2 - (r^2 + a^2 + \frac{2ma^2}{r})\dot{\phi}^2 \\ &\equiv \bar{a}\dot{t}^2 + 2\bar{c}\dot{t}\dot{\phi} - \bar{b}\dot{\phi}^2 - \frac{r^2}{\Delta}\dot{r}^2\end{aligned}$$

from which we calculate the conserved quantities (multiplied by additional factor of 1/2 for convenience)

$$A = (1 - \frac{2m}{r})\dot{t} + \frac{2am}{r}\dot{\phi} = \bar{a}\dot{t} + \bar{c}\dot{\phi}$$
$$B = \frac{2am}{r}\dot{t} - (r^2 + a^2 + \frac{2ma^2}{r})\dot{\phi} = \bar{c}\dot{t} - \bar{b}\dot{\phi}$$

Solving after $\dot{t}$ and $\dot{\phi}$ respectively yields

$$\dot{t} = (\bar{b}A + \bar{c}B)(\bar{a}\bar{b} + \bar{c}^2)^{-1}$$
$$\dot{\phi} = (\bar{c}A - \bar{a}B)(\bar{a}\bar{b} + \bar{c}^2)^{-1}$$

Noting that [5]

$$\begin{aligned}\bar{a}\bar{b} + \bar{c}^2 &= (1 - \frac{2m}{r})(r^2 + a^2 + \frac{2ma^2}{r}) + \frac{4a^2m^2}{r^2} \\ &= r^2 + a^2 - 2mr \\ &= \Delta\end{aligned}$$

finally gives us

$$\dot{t} = \frac{\bar{b}A + \bar{c}B}{\Delta} \tag{2}$$
$$\dot{\phi} = \frac{\bar{c}A - \bar{a}B}{\Delta} \tag{3}$$

We can use these two expressions two rewrite our Lagrangian

$$\begin{aligned}\mathcal{L} &= \bar{a}\dot{t}^2 + 2\bar{c}\dot{t}\dot{\phi} - \bar{b}\dot{\phi}^2 - \frac{r^2}{\Delta}\dot{r}^2 \\ &= \bar{a}(\frac{A^2\bar{b}^2 + 2\bar{b}\bar{c}AB + \bar{c}^2B^2}{\Delta^2}) + 2\bar{c}(\frac{\bar{b}A + \bar{c}B}{\Delta})(\frac{\bar{c}A - \bar{a}B}{\Delta}) - \bar{b}(\frac{\bar{c}^2A^2 - 2\bar{a}\bar{c}AB + \bar{a}^2B^2}{\Delta^2}) - \frac{r^2}{\Delta}\dot{r}^2 \\ &= \frac{A^2(\bar{a}\bar{b}^2 + \bar{b}\bar{c}^2) - B^2(\bar{a}\bar{c}^2 + \bar{a}^2\bar{b}) + 2AB(\bar{c}^3 + \bar{a}\bar{b}\bar{c})}{\Delta^2} - \frac{r^2}{\Delta}\dot{r}^2 \\ &= \frac{\bar{b}A^2 - \bar{a}B^2 + 2\bar{c}AB}{\Delta} - \frac{r^2}{\Delta}\dot{r}^2\end{aligned}$$

Where we have used the identity $\Delta = \bar{a}\bar{b} + \bar{c}^2$ in the last line. Inserting the definitions for $\bar{a}, \bar{b}$, $\bar{c}$ and Δ and rearranging gives us the radial equation

$$\dot{r}^2 - \frac{\mathcal{L}2m}{r} + \frac{B^2}{r^2} - \frac{2mB^2}{r^3} + \frac{\mathcal{L}a^2}{r^2} - \frac{a^2A^2}{r^2} - \frac{2ma^2A^2}{r^3} - \frac{4amAB}{r^3} = A^2 - \mathcal{L}$$

In the case of time-like geodesics we have $\mathcal{L} = 1$. We can further identify $E = \frac{A^2 - \mathcal{L}}{2}$ and $L = -B$ with E and L being the total energy per mass of the orbiting object and orbital angular momentum per mass respectively. We thus have in analogy with Newtonian mechanics

$$\frac{\dot{r}^2}{2} + V(r) = E \tag{4}$$

with

$$V(r) = \underbrace{-\frac{m}{r} + \frac{L^2}{2r^2}}_{Newton} \quad \underbrace{-\frac{mL^2}{r^3}}_{Schwarzschild} \quad \underbrace{-\frac{a^2E}{r^2} - \frac{ma^2(2E+1)}{r^3} + \frac{2am\sqrt{2E+1}L}{r^3}}_{Kerr} \tag{5}$$

As expected, we recover the Schwarzschild case for $a = 0$. It is interesting to note, that while the Schwarzschild correction is of $\mathcal{O}(r^{-3})$ the Kerr metric introduces additional terms of $\mathcal{O}(r^{-2})$. Thus the rotation of the gravitational source introduces relativistic effects which are of the same order in r as the Newtonian case.

2.2 Dimensional and calculational considerations

In order to examine the physical scales of our result we will momentarily restore our units

$$V(r) = -\frac{Gm}{r} + \frac{L^2}{2r^2} - \frac{GmL^2}{c^2r^3} - \frac{a^2E}{r^2} - \frac{Gma^2(2E+c^2)}{c^2r^3} + \frac{2aGm\sqrt{2E+c^2}L}{c^2r^3} \tag{6}$$

with $J = amc$ and $\mathcal{L} = c^2$. We observe that the Kerr terms scale with $\frac{a}{r}$ and $\frac{Gm}{c^2r}$ which correspond to the rotation and gravitational strength of the gravitational source respectively. Since the Schwarzschild contribution to the Mercurian perihelion shift is in accordance with the experimental data (GR: $\approx 43''$/century, Experiment: $42.56 \pm 0.94''$/century [6]) we expect $\frac{a}{r} \ll 1$ and $\frac{a^2}{r^2} \ll \frac{Gm}{c^2r}$ for the orbit of Mercury around the Sun[1]. Using the experimental value of $J_\odot = 1.92 \cdot 10^{41}$ kg m^2 s^{-1} [7] for the angular momentum of the Sun and using following values

$$M_\odot = 1.99 \cdot 10^{30} \text{ kg}$$
$$\tilde{a}_{mercury} = 5.79 \cdot 10^{10} \text{ m}$$

where $\tilde{a}_{mercury}$ is the semi-major axis of the orbit we get

$$\frac{a_\odot}{\tilde{a}_{mercury}} = 5.55 \cdot 10^{-9} \qquad \frac{Gm_\odot}{c^2\tilde{a}_{mercury}} = 2.55 \cdot 10^{-8}$$

in agreement with our expectations. We also have $E_{mercury}/c^2 = -1.28 \cdot 10^{-8}$ which indicates that motion of Mercury is well below the speed of light.

3 Perihelion shift in the far-field limit

In this section we derive the perihelion shift of a slowly orbiting object with $E \ll c^2$ for a slowly rotating ($\frac{a}{r} \ll 1$) and weak ($\frac{Gm}{c^2r} \ll 1$) gravitational source having the Kerr metric as the exterior vacuum solution.

We start by rewriting our radial equation (4) as a differential equation in ϕ rather than τ. We have

$$\dot{r} = \frac{\partial\phi}{\partial\tau}\frac{\partial r}{\partial\phi} \equiv \dot{\phi}r'$$

rearranging (4) and defining $\tilde{V}(r) = V(r) - E$ we have

$$\begin{aligned} r'^2 &= -2\frac{\tilde{V}(r)}{\dot{\phi}^2} \\ &\underset{(3)}{=} -2\frac{\Delta^2}{(\bar{c}\sqrt{2E+1} + \bar{a}L)^2}\tilde{V}(r) \end{aligned}$$

The full expression for the right hand side is rather complicated but since we are only interested in the slow rotating limit we will expand it in orders of a

$$r'^2 = \frac{2L^2mr - L^2r^2 + 2mr^3 + 2Er^4}{L^2} + \frac{8\sqrt{2E+1}mr^3(m+Er)}{L^3(2m-r)}a + \mathcal{O}(a^2)$$

We further note that the denominator of the second term can be expanded as well since $\frac{m}{r} \ll 1$

$$\frac{1}{L^3(2m-r)} = -\frac{1}{L^3r}(1 + \frac{2m}{r} + \mathcal{O}(\frac{m^2}{r^2}))$$

[1] As will be discussed below, the metric of the Sun is actually not given by the Kerr metric since it does not describe an arbitrarily rotating source. However, in the appropriate limiting case the two metrics do in fact coincide.

In leading order we thus have

$$r'^2 \approx \frac{2L^2mr - L^2r^2 + 2mr^3 + 2Er^4}{L^2} - \frac{8a\sqrt{2E+1}m^2r^2}{L^3} - \frac{8a\sqrt{2E+1}Emr^3}{L^3} \tag{7}$$

In order to make the solving of this equation more feasible we will introduce $u = \frac{1}{r}$ with $u' = -\frac{1}{r^2}r'$ leading to

$$u'^2 = 2mu^3 - u^2 + \frac{2m}{L^2}u + \frac{2E}{L^2} - \frac{8a\sqrt{2E+1}m^2}{L^3}u^2 - \frac{8a\sqrt{2E+1}Em}{L^3}u$$

Taking the derivative of this equation and dividing by $2u' \neq 0$ gives us the following second order non-linear differential equation:

$$u'' + u - \frac{m}{L^2} = 3mu^2 - \frac{8a\sqrt{2E+1}m^2}{L^3}u - \frac{4a\sqrt{2E+1}Em}{L^3} \tag{8}$$

We recover a similar differential equation as in the Newtonian case however with a right hand side unequal to zero from which we recognize the first term from the Schwarzschild treatment of this problem. We will assume that the deviations from Newtonian orbital motion will be small and we want to try to find a pertubative correction starting from the classical solution. Following a similar approach as in [8], we will introduce a parameter $p \in [0, 1]$ for that purpose and write a family of differential equations

$$u'' + u - \frac{m}{L^2} - p(3mu^2 - \frac{8a\sqrt{2E+1}m^2}{L^3}u - \frac{4a\sqrt{2E+1}Em}{L^3}) = 0 \tag{9}$$

For p=0 we regain the Newtonian equation of motion while for p=1 we get the full expression (8). We write the exact solution as a series expansion in p

$$u = u_0 + pu_1 + p^2u_2 + ...$$

where the first order correction is expressed via u_1. Plugging this expansion back into (9) we get

$$u_0'' + u_0 - \frac{m}{L^2} + p(u_1'' + u_1 - 3mu_0^2 + \frac{8a\sqrt{2E+1}m^2}{L^3}u_0 + \frac{4a\sqrt{2E+1}Em}{L^3}) + \mathcal{O}(p^2) = 0$$

and thus we get the two linear differential equations

$$u_0'' + u_0 - \frac{m}{L^2} = 0 \tag{10}$$

$$u_1'' + u_1 = 3mu_0^2 - \frac{8a\sqrt{2E+1}m^2}{L^3}u_0 - \frac{4a\sqrt{2E+1}Em}{L^3} \tag{11}$$

with (10) having the classical solution

$$u_0 = \frac{m}{L^2}(1 + \epsilon\cos\phi)$$

for $u_0(0) = r_{perihelion}^{-1}$, $u_0'(0) = 0$ and with ϵ being the eccentricity of the orbit. Using this solution for (11) gives us

$$u_1'' + u_1 = 3m\frac{m^2}{L^4}(\underbrace{1}_{I} + \underbrace{2\epsilon\cos\phi}_{II} + \underbrace{\epsilon^2\cos^2\phi}_{III}) - \frac{8a\sqrt{2E+1}m^2}{L^3}\frac{m}{L^2}(\underbrace{1}_{IV} + \underbrace{\epsilon\cos\phi}_{V}) - \underbrace{\frac{4a\sqrt{2E+1}Em}{L^3}}_{VI}$$

we can solve the different terms separately and get for $u_1(0) = u_1'(0) = 0$

$$\text{I, IV, VI} : u_1 \propto (1 - \cos\phi)$$
$$\text{II, V} : u_1 \propto \frac{1}{2}\epsilon\phi\sin\phi$$
$$\text{III} : u_1 \propto \epsilon^2(2 - \cos\phi - \cos^2\phi)$$

We note that the only aperiodic contributions come from II and V: $u_1'(2\pi) \neq 0$. Taking only the aperiodic part into consideration we write (for $p \to 1$)

$$u = \frac{m}{L^2}(1 + \epsilon\cos\phi) + (3m\frac{m^2}{L^4} - \frac{4a\sqrt{2E+1}m^2}{L^3}\frac{m}{L^2})\epsilon\phi\sin\phi$$

To finally calculate the perihelion shift we simply solve for $\Delta\phi$ in

$$\begin{aligned} u'(2\pi + \Delta\phi) &= -\frac{m}{B^2}\sin\Delta\phi + (3m\frac{m^2}{L^4} - \frac{4a\sqrt{2E+1}m^2}{L^3}\frac{m}{L^2})(\sin\Delta\phi + (2\pi+\Delta\phi)\cos\Delta\phi) \\ &\stackrel{!}{=} 0 \end{aligned}$$

for small $\Delta\phi$ we get

$$\begin{aligned} \Delta\phi &= \frac{2\pi(3m\frac{m}{L^2} - \frac{4a\sqrt{2E+1}m^2}{L^3})}{1 - 2(3m\frac{m}{L^2} - \frac{4a\sqrt{2E+1}m^2}{L^3})} \\ &\approx 2\pi(3m\frac{m}{L^2} - \frac{4am^2}{L^3}) \end{aligned}$$

or

$$\boxed{\Delta\phi \approx \frac{6\pi m^2}{L^2} - \frac{8\pi a m^2}{L^3}} \tag{12}$$

where we have used $L^2 \propto mr$ and $E \ll c^2$ in the last line.

4 Perihelion precession of Mercury

Contrary to the Schwarzschild metric, there is no Birkhoff's Theorem equivalent for the Kerr metric [4] [9]. This means that (5) only describes the effective potential of a body in the gravitational field of an uncharged, rotating Black hole and not an arbitrary rotating object.
However, in general, the metrics of such rotational objects (e.g. stars, planets) and the Kerr metric differ from each other in their respective higher order mulitpole expansion. This implies, that for large r (weak-field regime) the perihelion correction calculated from the Kerr metric is indeed the leading contribution. We have seen above that the relevant scales in the case of Mercury are much smaller than unity, so we expect the Kerr correction calculated above to be the leading contribution to the perihelion shift of Mercury induced by the Sun's rotation after all. A different approach, starting with a general metric in Post-Newtonian approximation and only considering the relevant multipole moments leads in fact to the same result (12)[10].

In order to calculate specific values for the case of Mercury we will identify $L = \sqrt{\tilde{a}Gm(1-\epsilon^2)}$ where $\tilde{a}$ refers to the semi-major axis of the orbital ellipse. Using $\epsilon_{mercury} = 0.206$ and the numerical values from section 2.2 we get for the first term in (12)

$$\frac{6\pi G^2 m_\odot^2}{c^2 L^2} \approx 5.01 \cdot 10^{-7} \quad (\hat{\approx} 42.9''/\text{century})$$

which is the famous result from 1916.
The second term yields

$$\frac{-8\pi a G^2 m_\odot^2}{cL^3} \approx -2.38 \cdot 10^{-11} \quad (\hat{\approx} -0.002''/\text{century})$$

Thus the calculated Kerr contribution to the Mercurian perihelion shift is well within the error of the experimental result of $42.56 \pm 0.94''$/century. Furthermore, our result is in agreement with previous results where the contribution of the rotation of the Sun to the Mercurian perihelion shift has been

calculated directly via the Lense-Thirring precession [11].

We can compare our result with the contribution to the perihelion shift coming from the Sun's quadrupole moment which is non-trivial due to the Sun's oblateness. It is given by [12]

$$(\Delta\phi)_Q = \frac{6\pi G^2 m_\odot^2}{L^2}\frac{J_2 r_\odot^2}{2L^2} \approx 2.97 \cdot 10^{-10} \quad (\hat{\approx} 0.025''/\text{century})$$

where we have used $J_2 = 2.0 \cdot 10^-7$ for the solar quadrupole moment. We thus see, that the Kerr contribution to the perihelion shift is roughly one order of magnitude smaller then the contribution from the Sun's quadrupole moment.

5 Reaching for the horizon

In this section we will gain insight into the strong field behaviour of time-like geodesics in the equatorial plane $\theta = \frac{\pi}{2}$. In particular, we want to study the existence and nature of orbits near the so-called *ergosphere*. The ergosphere describes the hypersurface at which the time-like Killing field $\frac{\partial}{\partial t}$ becomes space-like. This is tantamount to g_{tt} in (1) becoming negative. Thus the ergosphere radius in the equatorial plane is given by $r_e = 2m$.

5.1 Innermost stable circular orbits

In order to gain a qualitative understanding of orbits near the black hole we will plot the effective potential (5) for different values of L, E and a.[2] We will begin with the Schwarzschild case $a/m = 0$ and try to understand the orbital behaviour near the Schwarzschild event horizon $r/m = 2$. Fig. 1 shows a schematic effective potential for a fixed L where we can identify possible orbits and their characteristic radii by varying E. Note that the existence of bound orbits is predicated on the value of L.
A way to discuss the smallest possible bound orbits is to examine the radius of the innermost stable cirular orbit (ISCO). Since this orbit will also give us the smallest elliptical orbits, the ISCO will give us a characteristic length for the closest bound orbits in general. Fig. 2 shows the Schwarzschild effective potential for different L in a close region around the horizon. Stable circular orbits seem to emerge between $L/m = 2$ and $L/m = 4$. We can easily calculate r_{ISCO}

$$\left.\frac{dV_{a=0}(r)}{dr}\right|_{r=r_{ISCO}} = 0$$
$$\left.\frac{d^2V_{a=0}(r)}{dr^2}\right|_{r=r_{ISCO}} = 0$$

getting $r_{ISCO} = 6m$ (with $L/m = \pm 2\sqrt{3}$), as suggested by Fig. 2. In particular, this gives us the innermost radius of the accretion disk of a Schwarzschild black hole. Only for $|L/m| > 2\sqrt{3}$ the effective potential possesses a minimum and therefore allows for stable orbits in general. We note that the effective potential reaches zero from below in the limit of $r \to \infty$ since the dominant, Newtonian term is $\propto \mathcal{O}(-r^{-1})$. Thus, bound orbits only exist for $E < 0$. In particular we see from Fig. 2 that free falling objects with $\dot{r} = 0$ at $r \to \infty$ (or equivalently with $E = 0$) need a specific angular momentum of $L \geq 4$ to avoid the singularity. Note that the effective potential (5) differs for a photon since we would have $\mathcal{L} = 0$. Repeating the same calculation in that case would give us $r_{ISCO}^{ph} = 3m$.

[2] In the following we will use dimensionless units by promoting m to a physical constant. Parameters and values can be restored in their physical dimension by an appropriate combination of G, c and m: $L/m \to \frac{Lc}{Gm}$, $a/m \to \frac{ac^2}{Gm}$, $E \to E/c^2$, $V \to V/c^2$.

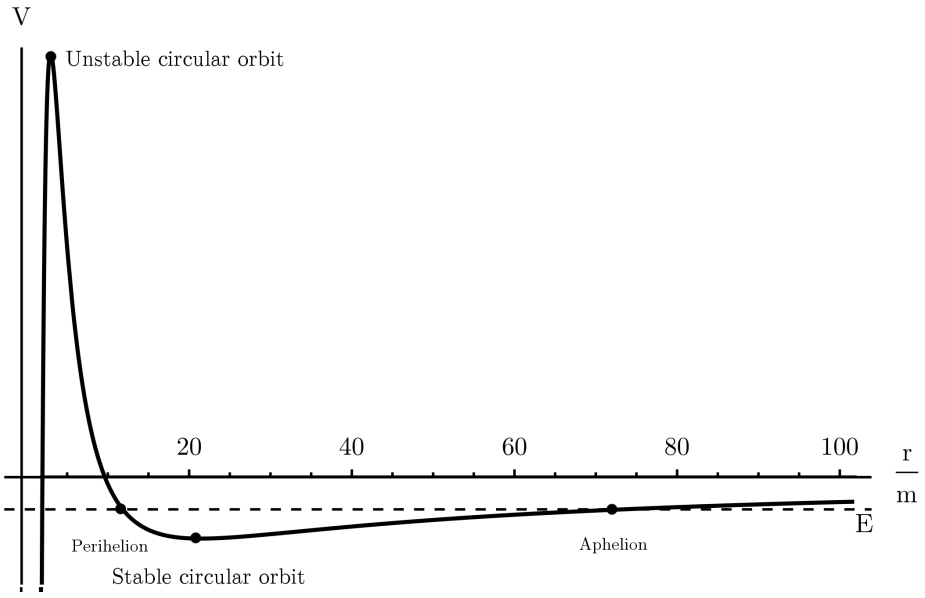

Figure 1: Schematic Schwarzschild effective potential which allows for bound orbits showing a possible elliptical orbit with energy E

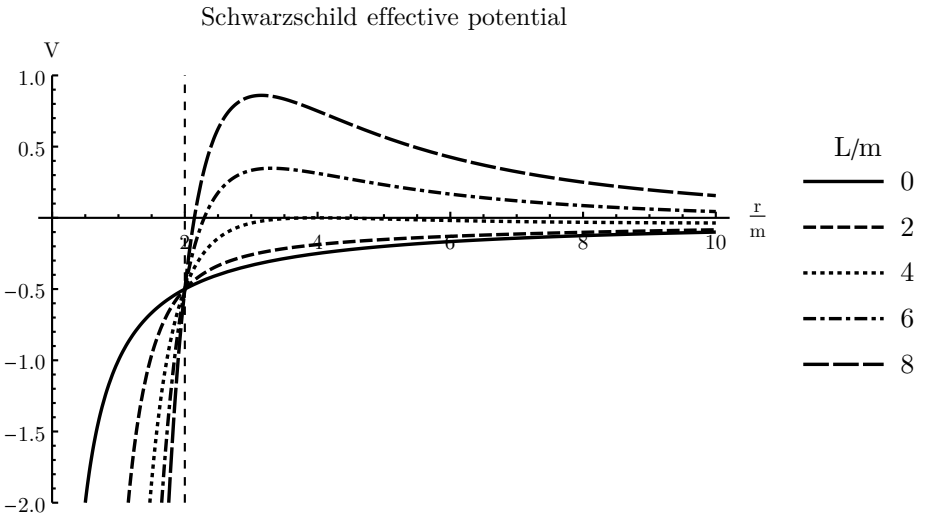

Figure 2: The near-field effective potential of the Schwarzschild metric for massive particles with different values of L/m.

We will now look at the case of $a/m \neq 0$. Note that in this case we have to consider negative values for L as well since (5) has a linear term in L breaking the angular symmetry of the spacetime. Fig. 3a and Fig. 3b show the effective potentials for a body orbiting with (direct, sgn(a)=sgn(L)) and against (retrograde, sgn(a)$\neq$ sgn(L)) the rotation of the black hole. The Kerr event horizon is given by $r = m + \sqrt{m^2 - a^2}$, characterized by a coordinate singularity in g_{rr} in (1), such that we have $a \in [0, m]$ for a Kerr black hole. Fig. 3 seems to suggest that the ISCO's differ for direct and retrograde orbital motions.

In this case the calculation of r_{ISCO} is more involved although it follows the same ideas as above. It is given by [13]

$$r_{ISCO} = m\big(3 + Z_2 \mp \sqrt{(3 - Z_1)(3 + Z_1 + 2Z_2)}\big)$$

with

$$Z_1 = 1 + (1 - \frac{a^2}{m^2})^{\frac{1}{3}}[(1 + \frac{a}{m})^{\frac{1}{3}} + (1 - \frac{a}{m})^{\frac{1}{3}}]$$
$$Z_2 = \sqrt{3\frac{a^2}{m^2} + Z_1^2}$$

where the plus and minus sign refer to orbital motion with and against the rotational direction of the black hole. Note that in principle the a dependenace of r_{ISCO} gives us a way to measure the angular momentum of a black hole via the measurement of the inner radius of the accretion disk. Fig. 4 shows the behaviour of r_{ISCO} for different values of a/m. As discussed in [13] the fact that is r_{ISCO} coincides with the event horizon for $a/m = 1$ is to be traced back to the singular behaviour of Boyer-Lindquist coordinates, in particular since the event horizon is a null hypersurface and thus doesn't allow for time-like geodesics. The ISCO for $a/m = 1$ is in fact a finite proper radial distance away from the horizon. Contrary to the Schwarzschild case, particles can orbit the Kerr black hole very close to the horizon ($a/m \approx 1$). This leads to interesting new phenomena and considerations absent in the Schwarzschild case, such as the idea that a rotating black hole can act as particle accelerator [14].

5.2 The ergosphere as the static limit

Another way of looking at the ergosphere is by realizing that observers with fixed spatial coordinate values (static observer) can only exist outside of it. This can be easily seen by reconsidering the phenomenon of the time-like coordinate becoming space-like at the ergosphere entry. A static observer has a four-velocity of $u^\mu \propto (1, 0, 0, 0)$ and as such seizes to be time-like at the ergosphere surface. Consequently, observers within the ergosphere can not be static. By considering an arbitrary four-velocity $u^\mu = (\dot{t}, \dot{r}, \dot{\phi}, 0)$ within the equatorial plane of the ergosphere and noting that for time-like geodesics we have

$$\begin{aligned} g_{\mu\nu}u^\mu u^\nu &= (1 - \frac{2m}{r})\dot{t}^2 + \frac{4am}{r}\dot{t}\dot{\phi} - \frac{r^2}{r^2 + a^2 - 2mr}\dot{r}^2 - (r^2 + a^2 + \frac{2ma^2}{r})\dot{\phi}^2 \\ &\equiv g_{tt}\dot{t}^2 + g_{t\phi}\dot{t}\dot{\phi} - g_{rr}\dot{r}^2 - g_{\phi\phi}\dot{\phi}^2 \\ &> 0 \end{aligned}$$

we see that $\dot{\phi} \neq 0$ and $\text{sgn}(\dot{\phi}) \stackrel{!}{=} \text{sgn}(a)$ from the second term since $g_{tt} < 0$ and all the other diagonal terms are strictly negative as well within the ergosphere. The same argument also holds for photons ($g_{\mu\nu}u^\mu u^\nu = 0$ in that case) and thus, within the ergosphere, every physical object is dragged along the rotational direction of the black hole. This phenomenon is known as *frame-dragging*. Fig. 5 shows the numerical solution[3] of the two cases where a particle approaches a black hole which rotates with and against the initial particle direction.

[3] All following numerical solutions have been obtained using *Mathematica*'s `NDSolve` and solving for dimensionless $r(\tau)$ and $\phi(\tau)$. Eqs.(3) and (4) have been used to obtain a second order differential equation in r and a first order differential equation in ϕ. In this case, the automated method selection of `NDSolve` has chosen `LSODA`, an integration procedure which automatically switches between stiff and non-stiff methods [15].

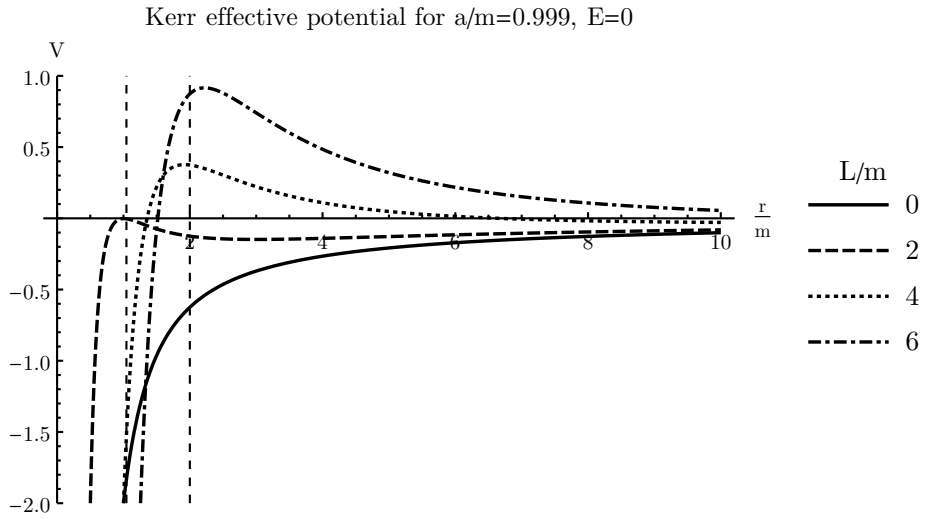

(a) direct

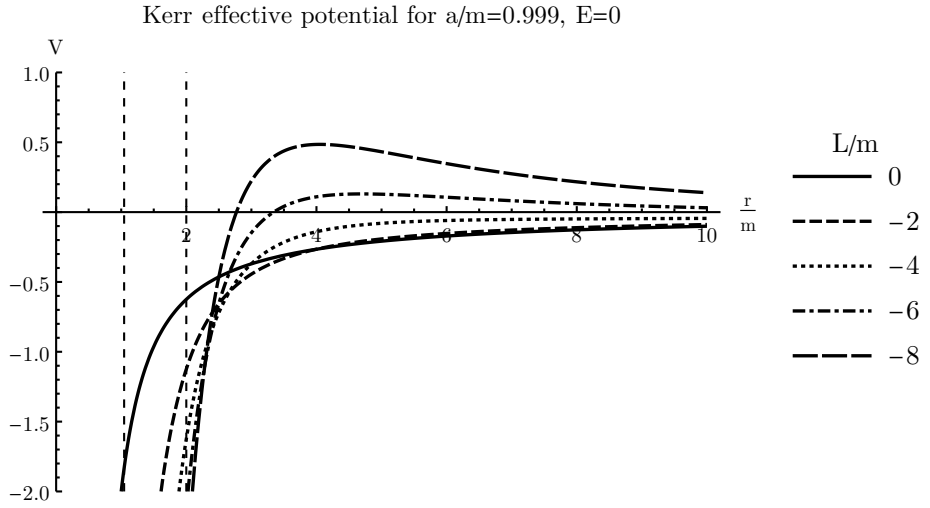

(b) retrograde

Figure 3: The effective potential of the Kerr metric with $a/m = 0.999$ and $E = 0$. The vertical inner and outer dotted lines denote the horizon and erogsphere radius respectively. Note the asymmetric behaviour for rising positive and negative values of L, exemplifying the dependence of geodesic motion on the rotational direction of the black hole (see also Fig. 5).

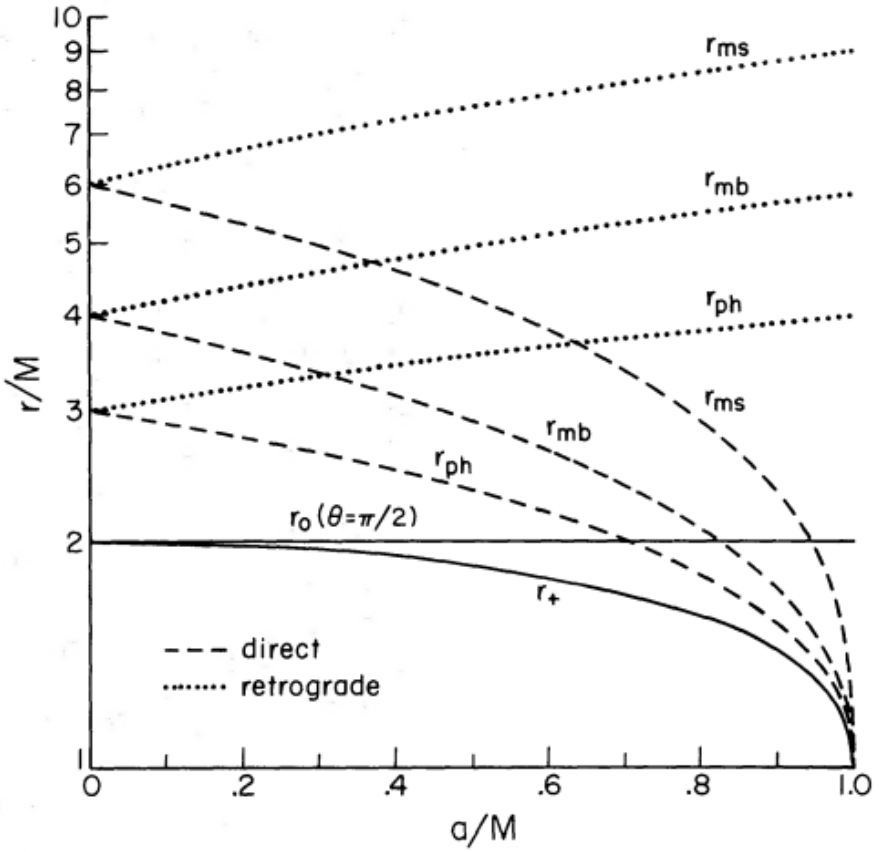

Figure 4: r_{ISCO} (denoted r_{ms} in the figure) in the equatorial plane of Boyer-Lindquist coordinates for different values of a/m for direct and retrograde orbital motion. r_{mb} and r_{ph} denote the closest unstable circular orbit and r^{ph}_{ISCO} respectively, whereas r_0 and r_+ denote the Ergosphere entry and the horizon [13]

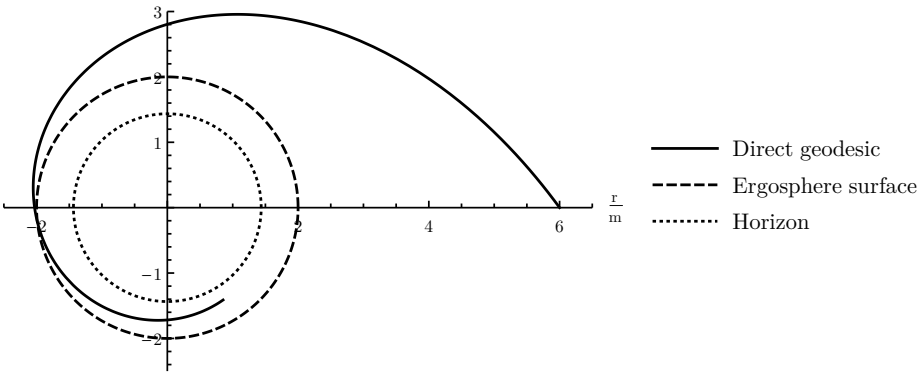

(a) Infalling direct geodesic with dimensionless parameters $E = -0.05$, $L = 2.3$, $a/m = 0.9$ and $\tau = 13$

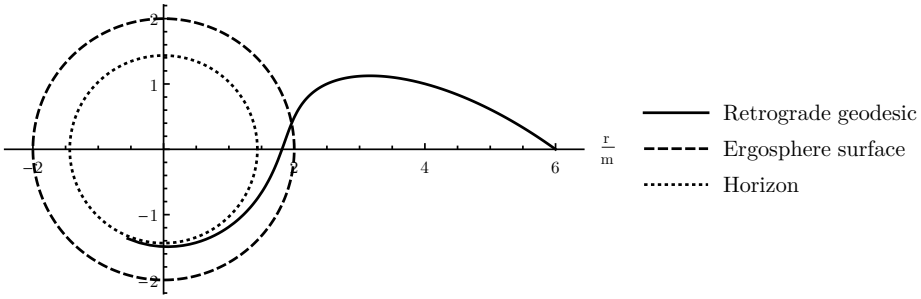

(b) Infalling retrograde geodesic with dimensionless parameters $E = -0.05$, $L = 2.3$, $a/m = -0.9$ and $\tau = 6.7$

Figure 5: Infalling direct and retrograde geodesics of massive particles approaching a rotating black hole. In the latter case, the particle is forced on to a path with the same rotational direction as the black hole before reaching the ergosphere.

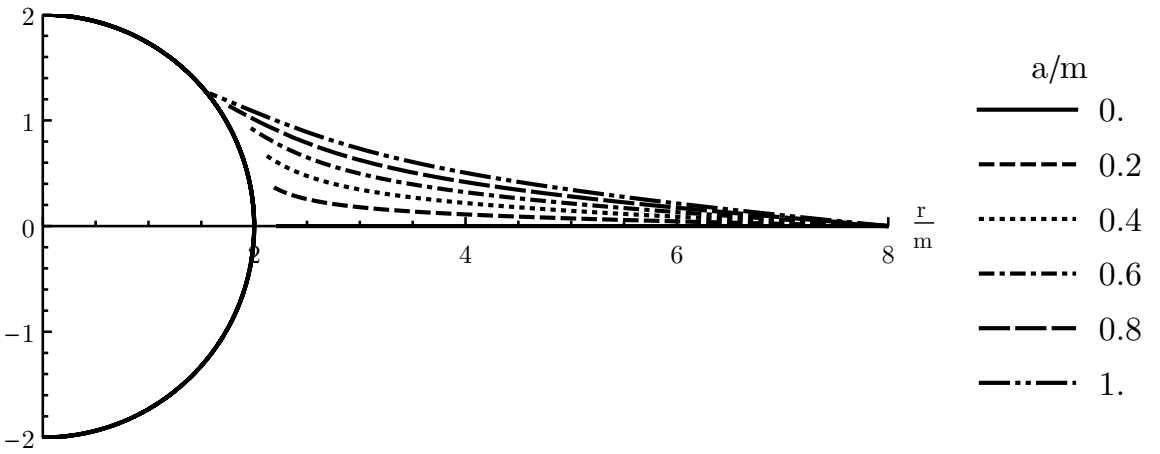

Figure 6: Frame-dragging effect for infalling massive particles reaching the ergosphere surface. Different values of a/m illustrate the warping of space in the rotational direction of the black hole. Dimensionless parameters used: $E = -0.05, L = 0, \tau = 10.7$

In the same manner, we expect a radially falling particle with $L = 0$ to acquire $d\phi/dt \neq 0$ while approaching the ergosphere. Using (2) and (3) we have

$$\frac{d\phi}{dt} = \frac{\dot{\phi}}{\dot{t}} \underset{L=0}{=} \frac{2am}{r^3 + a^2 r + 2a^2 m}$$

where $\mathrm{sgn}(d\phi/dt) = \mathrm{sgn}(a)$ is apparent and the dragging is indeed along the rotational direction of the black hole. Fig. 6 shows a numerical simulation of this case for different values of a/m.

5.3 Numerical perihelion shift

In this section, we will use numerical solutions to calculate the perihelion shift for arbitrary orbital parameters. In particular, we are interested in the perihelion shift of orbits close to the black hole.

The idea is to consider the numerically solutions of orbital motions (see footnote 3) and calculate the perihelion shift from the appropriate roots of the derivative of the interpolation function for $r(\tau)$. In order to verify the accuracy of this method we will begin with the case of Mercury and try to numerical determine the Schwarzschild perihelion shift. Fig. 7 depicts the procedure. We get a result of $\Delta\phi \approx 5.01 \cdot 10^{-7}$ in agreement with our pertubative calculation from section 4 [4]. Fig. 8 shows the numerical Mercurian perihelion shift together with results for slightly different L/m.

Next, we look at bound orbits close to the black hole. Fig. 9 shows bound orbits for $a/m \in \{0, 0.999, -0.999\}$ and for $L/m = 4.7$, $E = -0.01$ together with the computed numerical perihelion shift. We note that in the case of $a/m = -0.999$ the perihelion shifts over 2π which results in "inner loops" in the orbital motion (see Fig. 9c). We also note that the deviation from the Schwarzschild perihelion shift is negative for $a/m > 0$, as in our far-field result. Fig. 10 shows the numerical perihelion shift for $L/m \in [4, 7]$ which corresponds roughly to a perihelion/aphelion distance of $r_{perihelion} \approx 6m - 36m$ and $r_{aphelion} \approx 91m - 61m$ respectively. Note that the existence of bound orbits is dependant on the value of a/m, such that bound orbits do not exist for certain parameter values such as for $L/m = 4.5$ and $a = -0.999$.

[4] For the default settings of `NDSolve`, the numerical results for the Mercurian perihelion shift show dependence on the chosen initial conditions. In order to fix this, we have set `WorkinPrecision` → `30` in `NDSolve`.

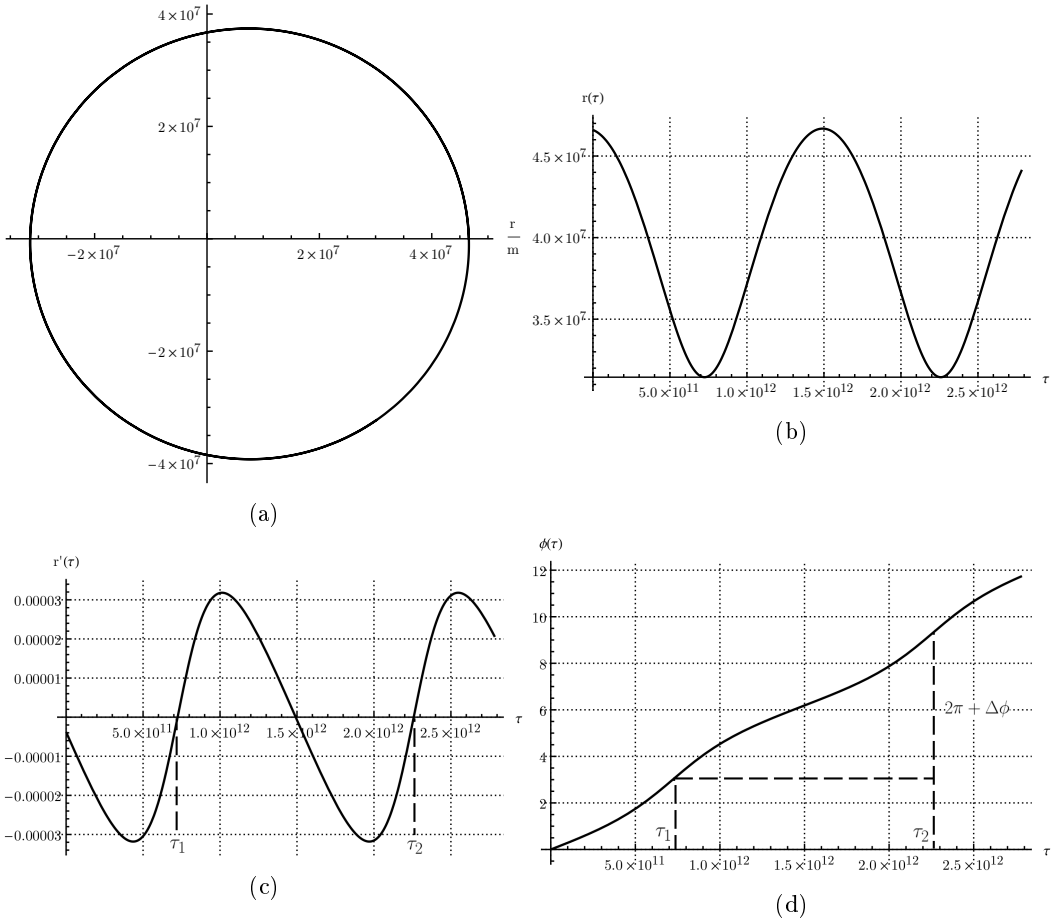

Figure 7: Finding the perihelion shift numerically for the case of Mercury using dimensionless parameters $E = -1.28 \cdot 10^{-8}$, $L = 6130$, $a/m = 0$ and $\tau = 1.8 \cdot (1.5 \cdot 10^{12})$. Numerical simulations of the Mercurian orbit for 1.8 revolutions are shown in (a). The interpolation function of the numerical results for $r(\tau)$ are shown in (b). In order to determine the perihelion shift we consider the distance between the relevant roots τ_1 and τ_2 of the the derivative of the interpolation function $r'(\tau)$ which is shown in (c). Finally, we determine the perihelion shift via $\phi(\tau_2) - \phi(\tau_1) = 2\pi + \Delta\phi$ in (d).

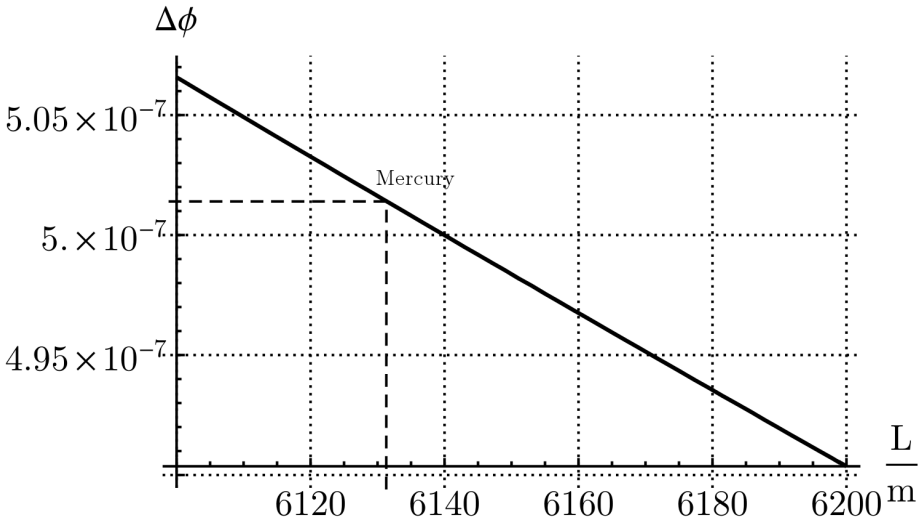

Figure 8: Perihelion shift as a function of L/m in the neighbourhood of the dimensionless specific angular momentum of Mercury $(L/m)_{mercury} = 6130$

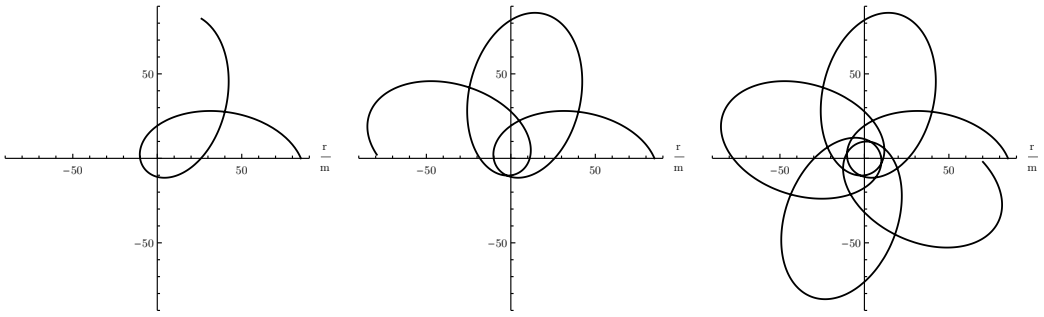

(a) Orbit around a Schwarzschild black hole with $E = -0.01$, $L/m = 4.7$ and $\tau = 9250$ yielding a numerical perihelion shift of $\Delta\phi = 1.50$

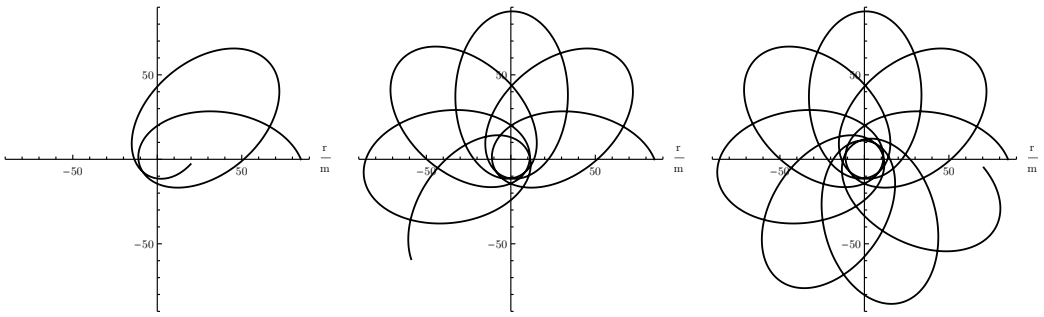

(b) Orbit around a Kerr black hole with $a/m = 0.999$, $E = -0.01$, $L/m = 4.7$ and $\tau = 15900$ yielding a numerical perihelion shift of $\Delta\phi = 0.85$

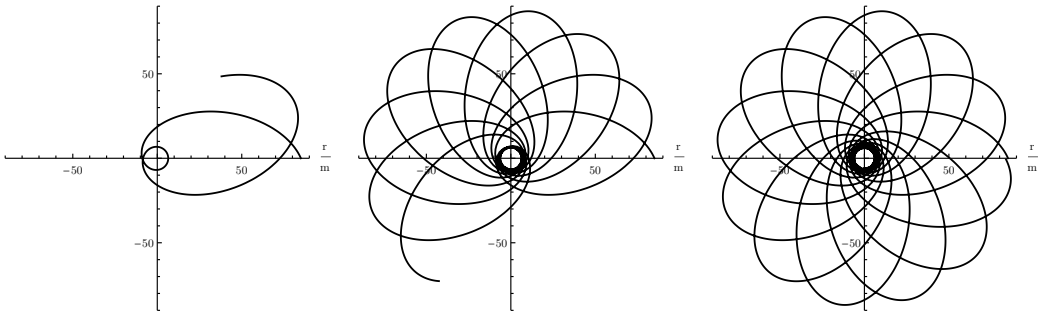

(c) Orbit around a Kerr black hole with $a/m = -0.999$, $E = -0.01$, $L/m = 4.7$ and $\tau = 27300$ yielding a numerical perihelion shift of $\Delta\phi = 6.80$

Figure 9: Time-evolution of closed orbits near a black hole for different values of a/m together with their numerical value for the perihelion shift per revolution.

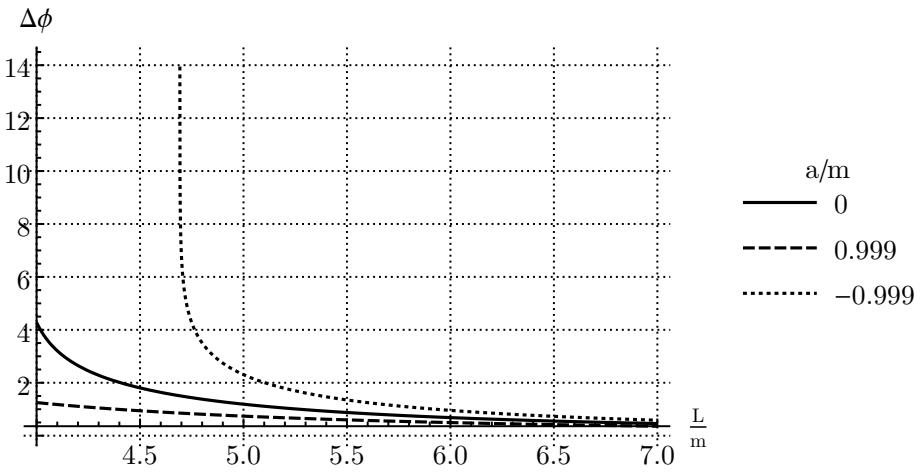

Figure 10: Numerical perihelion shift for orbits near a Kerr black hole with different values of a/m as a function of L/m. Dimensionless parameters used: $E = -0.01$

6 Conclusion

We have derived an effective potential (5) for radial movement in the equatorial plane from the Kerr metric and examined the Kerr contribution to the perihelion shift. We derived an analytical expression (12) for the case of slow movements and weak fields. In the case of Mercury, we have found that the rotation of the sun contributes $-0.002''$/century to the perihelion shift, which is in agreement with previous results using alternative approaches [10] [11]. We have also established a numerical method of calculating the perihelion shift in order to discuss near-field behaviour. The main results can be seen in Fig. 9 and Fig. 10 where the relation between direct and retrograde orbits of different sizes and the perihelion shift is depicted.

References

[1] K. Schwarzschild. *Über das Gravitationsfeld eines Massenpunktes nach der Einsteinschen Theorie. Sitzungsberichte der Königlich Preußischen Akademie der Wissenschaften (Berlin), 1916, Seite 189-196*, 1916.

[2] Albert Einstein. *Die Grundlage der allgemeinen Relativitätstheorie. Annalen Phys.*, 49(7): 769–822, 1916.

[3] Roy P. Kerr. *Gravitational Field of a Spinning Mass as an Example of Algebraically Special Metrics. Phys. Rev. Lett.*, 11:237–238, Sep 1963.

[4] Saul A Teukolsky. *The Kerr metric. Classical and Quantum Gravity*, 32(12):124006, 2015.

[5] Leonardo Gualtieri and Valeria Ferrari. *Black Holes in General Relativity, Lectures Notes Chapter 4*, 2011.

[6] G. M. Clemence. *The Relativity Effect in Planetary Motions. Reviews of Modern Physics*, 19: 361–364, October 1947.

[7] L. Iorio. *Constraining the Angular Momentum of the Sun with Planetary Orbital Motions and General Relativity. Solar Physics*, 281(2):815–826, Dec 2012.

[8] Victor Shchigolev. *Analytical Computation of the Perihelion Precession in General Relativity via the Homotopy Perturbation Method. Universal Journal of Computational Mathematics*, 3: 4549, 11 2015.

[9] M. Visser. *The Kerr spacetime: A brief introduction. ArXiv e-prints*, June 2007.

[10] Steven Weinberg. *Gravitation and Cosmology: Principles and Applications of the General Theory of Relativity*. Wiley, New York, NY, 1972.

[11] Lorenzo Iorio. *Advances in the Measurement of the Lense-Thirring Effect with Planetary Motions in the Field of the Sun. Scholarly Research Exchange*, 2008, 07 2008.

[12] S. Pireaux and J.-P. Rozelot. *Solar quadrupole moment and purely relativistic gravitation contributions to Mercury's perihelion advance. Astrophysics and Space Science*, 284(4):1159–1194, Jun 2003.

[13] J. M. Bardeen, W. H. Press, and S. A. Teukolsky. *Rotating Black Holes: Locally Nonrotating Frames, Energy Extraction, and Scalar Synchrotron Radiation. The Astrophysical Journal*, 178: 347–370, December 1972. doi: 10.1086/151796.

[14] Tomohiro Harada and Masashi Kimura. *Black holes as particle accelerators: a brief review. Classical and Quantum Gravity*, 31(24), 2014.

[15] Linda Petzold. *Automatic Selection of Methods for Solving Stiff and Nonstiff Systems of Ordinary Differential Equations. SIAM Journal on Scientific and Statistical Computing*, 4(1): 136–148, 1983.